Detection of hydrogen sulphide above the clouds in Uranus' atmosphere

Patrick G. J. Irwin[1], Daniel Toledo[1], Ryan Garland[1], Nicholas A. Teanby[2], Leigh N. Fletcher[3], Glenn S. Orton[4], & Bruno Bézard[5]

[1]*Department of Physics (Atmospheric, Oceanic and Planetary Physics), University of Oxford, Parks Rd, Oxford, OX1 3PU, UK.*

[2]*School of Earth Sciences, University of Bristol, Wills Memorial Building, Queens Road, Bristol, BS8 1RJ, UK.*

[3]*Department of Physics & Astronomy, University of Leicester, University Road, Leicester, LE1 7RH, UK.*

[4]*Jet Propulsion Laboratory, California Institute of Technology, 4800 Oak Grove Drive, Pasadena, CA 91109, USA*

[5]*LESIA, Observatoire de Paris, PSL Research University, CNRS, Sorbonne Universités, UPMC Univ. Paris 6, Université Paris-Diderot, Sorbonne Paris Cité, 5 place Jules Janssen, 92195 Meudon, France.*

Visible to near-infrared observations indicate that the cloud top of the main cloud deck on Uranus lies at a pressure level of between 1.2 and 3 bar. However, its composition has never been unambiguously identified, although it is widely assumed to be composed primarily of either ammonia (NH_3) or hydrogen sulphide (H_2S) ice. Here we present evidence of a clear detection of gaseous H_2S above this cloud deck in the wavelength region 1.57 – 1.59 μm

with a mole fraction of 0.4 – 0.8 ppm at the cloud top. Its detection constrains the deep bulk sulphur/nitrogen abundance to exceed 4.4 – 5.0 times the solar value in Uranus' bulk atmosphere, and places a lower limit on the mole fraction of H_2S below the observed cloud of $(1.0-2.5)\times 10^{-5}$. The detection of gaseous H_2S at these pressure levels adds to the weight of evidence that the principal constituent of 1.2 – 3-bar cloud is likely to be H_2S ice.

Introduction In the absence of any spectrally identifiable ice absorption features, the identity of the main component of the cloud in Uranus' atmosphere with cloud top pressure 1.2 – 3 bar[1–3] has long been a source of debate. The assumption that it is composed of either ammonia (NH_3) or hydrogen sulphide (H_2S) ice[3] is based on the expected presence at deeper pressures (~ 40 bar) of an ammonium hydrosulphide (NH_4SH) cloud. This cloud combines together in equal parts any available H_2S and NH_3, leaving the remaining more abundant molecule to condense alone at lower pressures[4]. Deeper in the atmosphere (20 – 40 bar), observations of Uranus and Neptune at microwave wavelengths (1 – 20 cm) with the Very Large Array (VLA)[5] found that there was a missing component of continuum absorption, which was concluded to be likely due to the pressure-broadened wings of H_2S lines with wavelengths of less than a few mm. The deep abundance of H_2S was estimated to be $10-30\times$ solar and this analysis further concluded, building upon previous studies[6,7], that the bulk S/N ratio must exceed $\sim 5\times$ the assumed solar ratio[8] in order that the bulk abundance of H_2S exceeds that of NH_3, leaving residual H_2S above the deeper NH_4SH cloud. Hydrogen sulphide is believed to be a significant component of all the giant planet atmospheres and has been detected *in situ* in Jupiter's deep atmosphere by the Galileo probe mass spectrometer[9] (and also in comets, both *in situ* and remotely[10,11]). However, it has never been unambiguously remotely detected in the atmospheres of any of the giant planets, aside from a possible debated detection in Jupiter's atmosphere following the impact of Comet Shoemaker-Levy 9 in 1994[12,13]. Hence, while H_2S is probably the source of the missing continuum absorption at microwave wavelengths in Uranus and Neptune's atmospheres, and is also probably the main component of the 1.2 – 3-bar cloud, it has never been unequivocally detected in Uranus' atmosphere to confirm this.

Detection of H_2S and NH_3 absorption features at thermal-IR wavelengths is very challenging due to the extremely cold atmospheric temperatures in Uranus' atmosphere, but at visible/near-infrared wavelengths, there are weak absorption bands that could potentially be detected in sunlight reflected from the cloud tops at wavelengths where the absorption of other gases is weak. The available line data for the key condensable volatiles in Uranus' atmosphere (i.e. CH_4, NH_3, H_2S) have recently been greatly improved[14,15] and, although these absorptions are weak, we looked to see whether we could detect these features in near-IR ground-based high resolution spectroscopic measurements.

Observations Observations of Uranus (with adaptive optics) were made with Gemini-North's Near-infrared Integral Field Spectrometer (NIFS) instrument in 2009/2010[16,17]. NIFS records $3'' \times 3''$ image 'cubes' with a pixel size of $0.103 \times 0.043''$, where each pixel is a spectrum covering, in the H-band, the wavelength range 1.476 – 1.803 μm with a spectral resolution of R = 5290. For this study we used observations recorded on 2nd November 2010 at approximately 06:00UT[17]. To minimise random noise we averaged the observations over seven 5×5 pixel boxes, indicated in Fig. 1 and listed in Table 1. We selected the wavelength region 1.49 – 1.64 μm for our analysis, comprising $n_y = 937$ spectral points. We initially set the noise at each wavelength to be the standard deviation of the data in these 5×5 pixel boxes. However, we found that we were not quite able to fit these spectra to a precision of $\chi^2/n_y \sim 1$ and attributed this to unknown deficiencies in our spectral modelling. We thus multiplied these errors by a single factor of 1.6 at all wavelengths (except for area '6', for which the variance was already sufficiently large) to account for these 'forward-modelling' errors. For our reference spectrum we chose the region close to the disc centre, centred at 15.3°N (Area '1'), but performed the same analysis for all other selected regions, reported in the supplementary material.

Analysis To model the observed spectra we used the NEMESIS[18] retrieval model, using the correlated-k approximation with 'k'-tables generated from the recently published WKLMC@80K+[14] line data for CH_4 and updated line data for H_2S and NH_3 from HITRAN2012[15]. The mean absorption strengths of CH_4, NH_3 and H_2S across the H-band wavelength range contained in these data (calculated at 100 K and 1 atm) are shown in Fig. 1. Our *a priori* vertical atmospheric profile was based on the 'F1' temperature profile, determined from HST/STIS and Voyager 2 observations[3]. This profile has a deep methane mole fraction of 4%[19], and has a varying relative humidity with height above the condensation level. The He:H_2 ratio was set to 0.131 and the profile includes 0.04% mole fraction of Ne[3]. To this profile we added NH_3 and H_2S, assuming arbitrary 'deep' mole fractions (i.e. above the putative NH_4SH cloud) of 0.1% for both, and limited their abundance to not exceed the saturated vapour pressure[20] in the troposphere as the temperature falls with height, adjusting the abundance of hydrogen and helium (keeping He:H_2 = 0.131) to ensure the mole fractions summed to unity at each pressure level. Figure 2 shows the modelled abundance profiles of the three condensible species falling with height. We can see that the saturated vapour pressure of H_2S at the pressure of the main clouds of Uranus (1.2 – 3 bar) is approximately 2000 times higher than that of NH_3. Hence, even though the peak NH_3 absorption strength in this spectral region is, from Fig. 1, ~ 100 times stronger than that of H_2S, we expect the absorption lines of H_2S to be far more visible due to the higher likely abundance of H_2S and also the lines of H_2S having maximum strength at wavelengths of minimum methane opacity (Fig. 1). The very low saturated vapour pressure of NH_3 at the 1.2–3 bar level in Uranus' atmosphere makes it likely that NH_3 would not have enough abundance to condense into a cloud with sufficient opacity at this level as has previously been noted[3].

We fitted the spectrum using a multiple-scattering model and modelled cloud opacity with a vertically continuous profile of particles (at 39 levels) with a Gamma size distribution of mean radius 1.0 μm and variance 0.05. This size distribution is typical of that assumed in previous analyses[2,21], but is an assumption and is not constrained by, for example, a microphysical model. In addition, the assumption that the particles have the same size distribution at all altitudes is an oversimplification since we would expect that in real clouds the particles would be smaller at higher altitudes. However, the primary objective of this study was to search for the spectral signature of H_2S gas, rather than to fit a sophisticated cloud model and we thus chose a model that would be simple and easy to fit. It should be noted that our simple cloud model is used to model not only the effects of the main 1.2 – 3 bar cloud, but also any CH_4 cloud opacity and any tropospheric/stratospheric haze opacity that may be present. In addition to fitting the cloud opacity at each level in the atmosphere, we also fitted the imaginary refractive index spectrum of the particles (assumed to be the same at all vertical levels) at nine wavelengths between 1.4 and 1.8 μm, reconstructing the real part of the refractive index spectrum using the Kramers-Kronig relation[21], assuming $n_{real} = 1.4$ at 1.6 μm. We constrained the imaginary refractive index spectrum to vary reasonably slowly with wavelength, to avoid degeneracy with the H_2S signal we were trying to detect (see Methods). Self-consistent extinction cross-sections, single-scattering albedos and phase functions were then computed at all wavelengths using Mie theory, with the phase functions approximated with Henyey-Greenstein functions (see Methods section). The total number of variable parameters in our retrieval was thus $n_x = 39 + 9 = 48$, and thus the total number of degrees of freedom, $n = n_y - n_x$ was 889.

Results Figure 3 shows our fit to the reference Uranus spectrum (Area '1' of Fig. 1 and Table 1) when H_2S and NH_3 absorption is neglected, using three different *a priori* values of the imaginary refractive index of 0.001, 0.01 and 0.1, respectively, at all wavelengths with an *a priori* error of $\pm 50\%$. We can see that reasonably good fits are achieved for all three cases, but that better fits are achieved with higher *a priori* values, with similar results for $n_i = 0.01$ and $n_i = 0.1$ ($\chi^2/n \sim 1.7$). For the $n_i = 0.001$ case, a poorer fit is achieved ($\chi^2/n \sim 1.9$) as the solution cannot move far enough away from the *a priori* to properly fit the spectrum. As a result the retrieved particles have low imaginary refractive index and so are more scattering, necessitating the cloud profile opacity to reduce quickly at pressures greater than 2–3 bar to prevent significant reflection from these levels. This is in stark contrast to the other two solutions, where n_i is much higher ($n_i \sim 0.06$), and where we find that the single-scattering albedo of the particles is $\varpi = 0.7 - 0.8$ and phase function asymmetry is $g \sim 0.7$ across the observed spectral range (Supplementary Fig.1).

These retrieved single-scattering albedo and phase-function asymmetry values agree very well with a limb-darkening analysis[16], which used these same Gemini/NIFS data smoothed to a lower resolution of FWHM = 0.004 μm and older, lower-resolution methane absorption k-distribution data[22], and also with an analysis of Keck and HST images[23], which recommended $\varpi = 0.75$ and $g = 0.7$. An important consequence of the low single-scattering albedo of the retrieved particles is that solar photons are quickly absorbed as they reach the cloud tops and so we do not see significant reflection from particles residing at pressures greater than 2–3 bar. This can be seen in the retrieved error bars for the cloud opacity profiles in Fig. 3 quickly relaxing back to their *a priori* value as the pressure increases and the profiles for the higher n_i values tending smoothly back to their *a priori* opacity/bar values. As a result, although we can clearly detect the cloud-top pressure at these wavelengths, we cannot tell where the base is and thus cannot differentiate between a vertically thin cloud based at 2–3 bar, or a cloud that extends vertically down to several bars with the same cloud-top pressure. We also note here that when the particles are constrained to be more scattering, the peak of cloud opacity is at a lower pressure than for the case with more absorbing particles. This phenomenon may help to explain why HST/STIS[3] retrievals, which assume the particles to be more scattering, find the cloud tops to be at lower pressures (1.2 bar) than retrievals near 1.5 μm[1,2], which assume more absorbing particles and find cloud tops at 2–3-bar.

Figure 4 compares our best fits to the observed reference spectrum (Area ‘1’ at 15.3°N) in the 1.56 – 1.60 μm region, including or excluding H_2S absorption. When H_2S absorption is not included, we find that there is a significant discrepancy between the measured and modelled spectra, giving χ^2/n = 1.71. This discrepancy is significantly reduced when H_2S absorption is included and

NEMESIS allowed to scale the abundance of H_2S, achieving a much closer fit with χ^2/n = 1.30. When H_2S absorption is not included, there are several peaks in the difference spectrum (Fig. 4) that match perfectly the effect of including or excluding this gas in the spectral calculation. We examined the correlation between the expected H_2S signal and this difference spectrum between 1.57 and 1.60 μm, and found a Pearson correlation coefficient of 0.718 (indicating a strong correlation) and a Spearman rank correlation coeffcient of 0.602, with a two-sided significance value of D = 6.88×10^{-20}, which equates to a 9-σ-level detection. We also tested the effect on the calculated spectrum of including or excluding 100% relative humidity of ammonia (NH_3), but found that this was completely undetectable due to ammonia's extremely low abundances at these temperatures. In case the ammonia abundance in Uranus' atmosphere is in reality highly supersaturated, we also tested the effect on the calculated spectrum of supersaturating NH_3 by factor of 1000, also shown in Fig. 4. However, we found that the absorption features of NH_3 do not coincide at all well with the difference spectrum, with correlation coefficients of only 0.271 (Pearson) and 0.256 (Spearman), respectively. We thus conclude that NH_3 is not the source of the missing absorption. The correlation between the spectral discrepancy of the fit, when H_2S is neglected, and the differences between the modelled spectra when H_2S or NH_3 absorption is added are shown in Supplementary Fig. 2.

The retrieved relative humidity of the H_2S profile needed to match the observed absorption features was $113 \pm 12\%$. Since the mole fraction of H_2S decreases rapidly with height, this scaling factor is strongly weighted by the abundance of H_2S just above the cloud tops, i.e. at 2–3 bar and found to be 0.47 ppm, but is consistent with the H_2S profile having 100% relative humidity in this region. However, this conclusion depends upon both the assumed temperature profile, which sets the saturated vapour pressure, and also the assumed methane profile, which affects the retrieved cloud-top pressure and thus the peak pressure level (and thus local temperature) of sensitivity to H_2S. To test these effects we repeated our retrievals using a vertical profile of temperature and abundance estimated from Spitzer[24], which has a lower CH_4 abundance of 3.2%, compared with 4% for the 'F1' profile[3], but is slightly warmer at pressures greater than 1 bar, resulting in higher saturated vapour pressures of H_2S. As might be expected, the lower CH_4 abundance of this profile led to the retrieved cloud opacity peaking at slightly higher pressures to achieve the required column abundance of CH_4 (Table 1) and the retrieved H_2S relative humidity at the deeper cloud tops in the warmer atmosphere was only $16 \pm 2\%$. Since it is not clear which of these two profiles is more reliable, (although the 'F1' profile was found to be inconsistent with Spitzer observations[24]) it can be seen that although we clearly detect the presence of H_2S at Uranus' cloud tops, it is difficult to quantitatively determine its relative humidity. However, we can see from Table 1 that there is very good correspondence between the retrieved values of column abundance of H_2S above the clouds for the two temperature profiles and also between the retrieved mole fraction of H_2S at the cloud-top pressure level of $(4.7 \pm 0.5) \times 10^{-7}$ for the 'F1' profile and $(4.3 \pm 0.5) \times 10^{-7}$ for the Spitzer profile, where we have propagated the relative humidity retrieval errors.

Table 1 and Supplementary Figs. 3 – 11 show our fits at the other test points on Uranus' disc, indicated in Fig. 1. At all locations except in Uranus' northern polar 'cap' feature we found a clear improvement in our fit to the spectra when H_2S absorption is included, indicating the presence of H_2S at the cloud tops (Table 1), with well defined column abundances above the cloud of $(2-5)\times10^{19}$ molecule cm^{-2} and cloud-top mole fractions of 0.4 – 0.8 ppm. All but one of the chosen points were on the central meridian, to keep the zenith angle as low as possible to minimise the computation time of our multiple scattering code, which uses more Fourier components in the azimuth decomposition direction as the zenith angle increases to maintain accuracy. However, point '2' was chosen to be at roughly the same latitude as our reference area, but off the central meridian and closer to the limb to check that our retrieval was robust against zenith angle changes, which was found to be the case. The absence of a clear H_2S signature near Uranus' north pole seems to indicate lower H_2S above the clouds in this region, in the same way that microwave observations found that the polar regions were depleted in microwave absorbers (H_2S and NH_3) at depth[6]. The abundance of methane above the clouds is also known to be reduced at these latitudes[3,19]. Alternatively, it could also be that the H_2S signal is masked by increased abundance of tropospheric haze, but Table 1, which lists a haze 'index', given by the observed radiance in a methane absorbing band divided by the radiance at continuum wavelengths, does not suggest that the polar region is particularly affected by overlying haze. However, to explore this further requires a detailed examination of spectra in the polar regions, which is beyond the scope of this paper.

Discussion If we could be sure that the main observed cloud deck was vertically thin and composed of H_2S ice, then we could constrain the abundance of H_2S below it by equating the cloud base to the condensation level. However, the low retrieved single-scattering albedo of the cloud particles means that we cannot tell between whether we are seeing a vertically thin cloud based at 2–3 bar or just the top of a vertically extended cloud that extends to several bars. Instead, our detection of H_2S can be used to give a lower limit on its abundance below the observed cloud.

Assuming the main cloud is made of H_2S ice, is vertically thin and is based at 3 bars, and that the STIS/Voyager-2 'F1' temperature profile[3] we have assumed is correct, the saturated mole fraction of H_2S at the 3-bar level (where the temperature is 116.1K) is estimated to be 1.1×10^{-5}. Alternatively, using the Spitzer profile[24], the saturated vapour mole fraction at the 3-bar level (where the temperature is 119.5 K) is 2.5×10^{-5}. Hence, we can conclude that the mole fraction of H_2S at pressures > 3 bar, immediately below the clouds must be $> (1.0 - 2.5) \times 10^{-5}$. We can compare this with the expected abundances of H_2S and NH_3 from microwave VLA studies[5–7], who found the abundance of H_2S to be 10 – 30 $\times$ solar, and S/N $> \sim$ 5, assuming solar abundances[8] of H_2S/H_2 = 3.76 $\times 10^{-5}$ and NH_3/H_2 = 1.74 $\times 10^{-4}$ (giving N/S = 4.6). Using these values, $10\times$solar H_2S and $2\times$solar NH_3 would give a residual mole fraction of H_2S above a deeper NH_4SH cloud of at least 3×10^{-5}, while for $30\times$solar H_2S and $6\times$solar NH_3, the expected residual H_2S mole fraction increases to 9×10^{-5}. Both these values are significantly greater than our estimated minimum residual abundance, but are consistent with it and may suggest that the base of the cloud lies at pressures greater than 3 bar. A more recent analysis of Spitzer Uranus observations[24] suggests a residual H_2S mole fraction of 1.5×10^{-5} in order to reconcile the millimetre spectrum with the temperature profile derived from Spitzer, which is much closer to our estimate. Interpolating to the pressure levels in our assumed 'F1' temperature-pressure profile[3] where the VLA and Spitzer estimates of residual H_2S abundance are equal to the saturated vapour pressure abundances we deduce that the base of the main cloud must lie at a pressure of 3.1 – 4.1 bar. Alternatively, if we assume the Spitzer temperature-pressure profile[24], we find a pressure range 2.8 – 3.7 bar. The fact that we detect H_2S at all at Uranus' cloud tops confirms that the deep abundance of H_2S must exceed that of NH_3 and hence that S/N $> 4.6\times$ solar for the solar abundance ratios[8] assumed by the VLA study[5,6]. We note, however, that there are other, more recent estimates of the solar abundance ratios, for which the solar N/S value varies from 4.4[25] to 5.0[26]. Hence, to ensure that the deep abundance of H_2S exceeds that of NH_3 we conclude that the S/N ratio in Uranus' bulk atmosphere exceeds 4.4–5.0 × solar. The clear detection of gaseous H_2S above Uranus' clouds leads us to conclude that H_2S ice likely forms a significant component of the main clouds at 1.2 – 3 bar. To our knowledge the imaginary refractive index spectrum of H_2S ice has not been measured and hence we cannot directly verify if our retrieved refractive index spectrum is consistent with H_2S ice. However, very large imaginary refractive indices, such as we retrieve, are absent in the measured complex refractive index spectra of H_2O, CH_4 and NH_3 ices. This suggests that if Uranus' main clouds are indeed formed primarily of H_2S ice, the particles may not be pure condensates, but may be heavily coated or mixed with photochemical products drizzling down from the stratosphere above, lowering their single-scattering albedos.

1 References

1. de Kleer, K., Luszcz-Cook, S., de Pater, I., Ádámkovics, M. & Hammel, H.B. Clouds and aerosols on Uranus: Radiative transfer modeling of spatially-resolved near-infrared Keck spectra. *Icarus* **256**, 120 – 137 (2015).

2. Irwin, P.G.J., de Bergh, C., Courtin, R., Bézard, B., Teanby, N.A., Davis, G.R., Fletcher, L.N., Orton, G.S., Calcutt, S.B., Tice, D. & Hurley, J. The application of new methane line absorption data to Gemini-N/NIFS and KPNO/FTS observations of Uranus' near-infrared spectrum.

Icarus **220**, 369 – 382 (2012b).

3. Sromovsky, L.A., Fry, P.M., & Kim, J.H. Methane on Uranus: The case for a compact CH_4 cloud layer at low latitudes and a severe CH_4 depletion at high latitudes based on a re-analysis of Voyager occultation measurements and STIS spectroscopy. *Icarus* **215**, 292 – 312 (2011).

4. Weidenschilling, S.J. & Lewis, J.S. Atmospheric and cloud structures of the Jovian planets. *Icarus* **20**, 465 – 76 (1973).

5. de Pater, I.,Romani, P.N. & Atreya. S.K. Possible microwave absorption by H_2S gas in Uranus' and Neptune's atmospheres. *Icarus* **91**, 220 – 233 (1991).

6. de Pater, I.,Romani, P.N. & Atreya. S.K. Uranus' deep atmosphere revealed. *Icarus* **82**, 288 – 313 (1989).

7. de Pater, I. & Massie, S. Models of the millimeter-centimeter spectra of the giant planets. *Icarus* **62**, 143 – 171 (1985).

8. Cameron, A.G.W. Elemental and Nuclidic Abundances in the Solar System. In *Essays in Nuclear Astrophysics* (C. A. Barnes, D. D. Clayton, and D. N. Schramm, Eds.), pp. 23-43, Cambridge Univ. Press, London/New York (1982).

9. Niemann, H.B., et al. The composition of the jovian atmosphere as determined by the Galileo probe mass spectrometer. *J. Geophys. Res.* **103**, 22831 – 22845 (1998).

10. Boissier, J., Bockelée-Morvan, Biver, N., Crovisier, J., Despois, D., Marsden, B.G. & Moreno, R. Interferometric imaging of the sulfur-bearing molecules H_2S, SO and CS in comet C/1995 O1 (Hale-Bopp). *Astron. Astrophys.* **475**, 1131 – 1144 (2007).

11. Eberhardt, P., Meier, R., Krankowsky, D. & Hodges, P.R. Methanol and hydrogen sulfide in comet P/Halley. *Astron. Astrophys.* **288**, 315 – 329 (1994).

12. Noll, K.S., McGrath, M.A., Trafton, L.M., Atreya, S.K., Caldwell, J.J., Weaver, H.A.,Yelle, R.V., Barnet, C. & Edgington, S. HST Spectroscopic observations of Jupiter after the collision of Comet Shoemaker-Levy 9. *Science* **267**, 1307 – 1313 (1995).

13. Lellouch, E. Chemistry induced by the impacts: Observations. IAU Colloquium 156; *Proceedings of the Space Telescope Science Institute Workshop*, held in Baltimore, Maryland, May 9–12, 1995. Eds.: Keith S. Noll, Harold A. Weaver, Paul D. Feldman, Cambridge University Press, p. 213 (1996).

14. Campargue, A., Leshchishina, O., Wang, L., Mondelain, D. & Kassi, S. The WKLMC empirical line lists (5852 – 7919 cm^{-1}) for methane between 80 K and 296 K: “Final” lists for atmospheric and planetary applications. *J. Molec. Spectrosc.* **291**, 16 – 22 (2013).

15. Rothman, L.S., Gordon, I.E., Babikov, Y., Barbe, A., Benner, D.C., Bernath, P.F., et al. The HITRAN2012 molecular spectroscopic database, *J.Q.S.R.T.* **130**, 4 – 50 (2013).

16. Irwin, P.G.J., Teanby, N.A., Davis, G.R., Fletcher, L.N., Orton, G.S., Tice, D. & Kyffin, A. Uranus’ cloud structure and seasonal variability from Gemini-North and UKIRT observations. *Icarus* **212**, 339 – 350 (2011).

17. Irwin, P.G.J., Teanby, N.A., Davis, G.R., Fletcher, L.N., Orton, G.S., Calcutt, S.B., Tice, D. & Hurley, J. Further seasonal changes in Uranus' cloud structure observed by Gemini-North and UKIRT. *Icarus* **218**, 47 – 55 (2012a).

18. Irwin, P.G.J., Teanby, N.A., de Kok, R., Fletcher, L.N., Howett, C.J.A., Tsang, C.C.C., Wilson, C.F., Calcutt, S.B., Nixon, C.A. & Parrish, P.D. The NEMESIS planetary atmosphere radiative transfer and retrieval tool. *J.Q.S.R.T.* **109**, 1136 – 1150 (2008).

19. Karkoschka, E. & Tomasko, M.The haze and methane distributions on Uranus from HST-STIS spectroscopy. *Icarus* **202**, 287–309 (2009).

20. Fray, N. & Schmitt, B. Sublimation of ices of astrophysical interest: A bibliographic review. *Plan. Space. Sci.* **57**, 2053 – 2080 (2009).

21. Irwin, P.G.J., Tice, D.S., Fletcher, L.N., Barstow, J.K., Teanby, N.A., Orton, G.S. & Davis, G.R. Reanalysis of Uranus' cloud scattering properties from IRTF/SpeX observations using a self-consistent scattering cloud retrieval scheme. *Icarus* **250**, 462 – 476 (2015).

22. Karkoschka, E. & Tomasko, M. Methane absorption coefficients for the jovian planets from laboratory, Huygens, and HST data. *Icarus* **205**, 674 – 694 (2010).

23. Sromovsky, L.A. & Fry, P.M. Spatially resolved cloud structure on Uranus: Implications of near-IR adaptive optics imaging. *Icarus* **192**, 527 – 557 (2007).

24. Orton, G.S., Fletcher, L.N., Moses, J.I., Mainzer, A., Hines, D., Hammel, H., Martin-Torres, J., Burgdorf, M., Merlet, C. & Line, M.R. 1. Mid-Infrared spectroscopy of Uranus from the

Spitzer Infrared Spectrometer: Determination of the mean temperature of the upper troposphere and stratosphere. *Icarus* **243**, 494 – 513 (2014).

25. Grevesse, N., Asplund, M. & Sauval, A.D. The solar chemical composition. *Space Sci. Rev.* **130**, 105 – 114 (2007).

26. Lodders. K. Solar System Abundances of the Elements, in *Principles and Perspectives in Cosmochemistry*, Astrophysics and Space Science Proceedings, ISBN 978-3-642-10351-3. Springer-Verlag Berlin Heidelberg, p. 379 (2010).

Correspondence Correspondence and requests for materials should be addressed to Patrick G. J. Irwin (email: patrick.irwin@physics.ox.ac.uk).

Acknowledgements We are grateful to the United Kingdom Science and Technology Facilities Council for funding this research and also to our support astronomers: Richard McDermid and Chad Trujillo (2009, 2010). The Gemini Observatory is operated by the Association of Universities for Research in Astronomy, Inc., under a cooperative agreement with the NSF on behalf of the Gemini partnership: the National Science Foundation (United States), the Science and Technology Facilities Council (United Kingdom), the National Research Council (Canada), CONICYT (Chile), the Australian Research Council (Australia), Ministério da Ciência e Tecnologia (Brazil) and Ministerio de Ciencia, Tecnología e Innovación Productiva (Argentina). We thank Larry Sromovsky for providing the code used to generate our Rayleigh-scattering opacities. Glenn Orton was supported by NASA funding to the Jet Propulsion Laboratory, California Institute of Technology. Leigh Fletcher was supported by a Royal Society Research Fellowship at the University of Leicester.

Author Contributions P.G.J.I. wrote the proposal to make the original observations and reduced the data and re-analysed it using the NEMESIS code; B.B. and R.G. assisted in identifying and validating the line data used. G.A.O. provided the Spitzer T-P profile used. L.N.F., N.A.T., D.T., and all co-authors contributed to the analysis, interpretation of the results, and all co-wrote the final paper.

Competing Interests The authors declare that they have no competing financial interests.

2 Figure Legends

Figure 1. The appearance and spectrum of Uranus at the near-infrared wavelengths observed by Gemini/NIFS and associated absorption spectra of CH_4, NH_3 and H_2S. Panel A: The appearance of Uranus at 1.55 μm (low methane absorption, showing reflection for cloud/haze at all vertical levels), observed with Gemini/NIFS on 2nd November 2010 at approximately 06:00UT, showing the position of the seven 5×5 pixel test areas picked for retrieval analysis. Panel B: The appearance of Uranus at 1.62 μm (high methane absorption, showing reflection from upper atmospheric haze only). Panel C: Reference spectrum of Uranus[16] analysed in this study, averaged over area '1' just north of the equator, near the disc centre, with a mean latitude of 15.3°N, and error estimates shown in grey. Panel D: Mean strength listed in the k-distribution tables used in this study across the Gemini/NIFS spectral range. These absorption tables were generated from the WKLMC@80K+[14] database for CH_4, and from HITRAN2012[15] for H_2S and NH_3. These mean absorption coefficients have been computed at a temperature of 100 K and pressure of 1 atm, similar to conditions found at the tops of Uranus' main visible clouds. Note that for NH_3, the linedata in HITRAN2012 terminate at 1.587 μm, roughly half way through the H_2S absorption band.

Figure 2. Assumed pressure variation of temperature (left-hand panel) and condensible abundances (right-hand panel) assumed in this study for Uranus. The temperature-pressure profile is based on the 'F1' profile[3]. The vertical variation of the CH_4 abundance is as described in the text. The abundances of NH_3 and H_2S have simply been limited by their saturation vapour pressures.

Figure 3. Fits to average Gemini/NIFS observation of Uranus, made on 2nd November 2010 at 15.3° N, using three different assumptions for the *a priori* imaginary refractive index spectrum, and excluding H_2S and NH_3 absorption. The red lines shows the results using $n_i = 0.001 \pm 0.0005$, the black lines shows the results using $n_i = 0.01 \pm 0.005$, while the blue lines show the results using $n_i = 0.1 \pm 0.05$. Panel a) shows the fits to the measured spectra, panel b) shows the difference between the observed and modelled spectra. Panel c) shows the fitted imaginary refractive index spectra of the one type of particle assumed right hand plot, while panel d) shows the fitted cloud profiles (opacity/bar at 1.6 μm). In panels c) and d) the *a priori* value and range is marked in light grey, while the error range on the retrieved quantities is indicated in darker grey. The χ^2/n of the fits is also shown in panel a).

Figure 4. Fits to the co-added Gemini/NIFS observation of Uranus in the wavelength range 1.56 – 1.6 μm. In the top plot, the observed reflectivity spectrum and estimated error is shown in grey, the fitted spectrum when H_2S absorption is not included is shown in red, while the fitted spectrum when H_2S absorption **is** included is shown in black. The bottom plot shows the differences between these fits and the observed spectrum using the same colours (i.e. red when H_2S absorption is not included and black when it is), with the error range again shown in grey. The

blue line in the bottom plot shows how the calculated spectrum for the fit when H_2S absorption is not included (i.e. red line in the top plot) changes when H_2S absorption is added (leaving all other fitted parameters unchanged), assuming a profile with 100% relative humidity (RH). The cyan line shows how the calculated spectrum changes when NH_3 absorption is added, leaving all other fitted parameters unchanged, assuming a profile with 1000 times the *a priori* NH_3 profile with 100% RH.

Methods

Spectral Data Sources The main gaseous absorber in the H-band (1.4 – 1.8 μm) in Uranus' spectrum is methane. The best available source of methane line data at low temperature in this range is the WKLMC@80K+[14] line database, which contains the positions, strengths, lower-state energies and empirical estimates of the rotational quantum number J, of lines measured at 80K and 296K. These lines are improved over the WKMC@80[27] database, previously used to analyse the Gemini/NIFS observations reanalysed here for Uranus[2] as they include extra lines that were detected at 296K, but not at 80K, and we have further improved our assignment of line widths, as described below. For the lines detected at 296K, but not 80K, lower state energies were defined so as to yield an intensity at 80 K just below the measurement sensitivity threshold. Hence, the contribution of these lines at cold temperatures bears significant uncertainty. For the lines detected at 80K, but not 296 K, the lower state energies were arbitrarily set to -1.0 cm^{-1}. These line data were converted to HITRAN format, using the listed strengths at 296 K directly for lines observed at both 80 K and 296 K, and for lines observed only at 80K, we extrapolated their strengths to 296 K using the listed arbitrary lower state energy of -1.0 cm^{-1} and total partition function (rotational + vibrational) provided as part of HITRAN2012[15]. The spectral range covered by these data is 5852 – 7919 cm^{-1} (1.262 – 1.709 μm). These measurements were made for "natural" methane gas, for which the CH_3D/CH_4 ratio is estimated[14] to be 5×10^{-4} . This is not suitable for calculations in Uranus' atmosphere, for which the most precise estimate[28] of CH_3D/CH_4 is $(2.96^{+0.71}_{-0.64}) \times 10^{-4}$ (using an isotopic enrichment factor[29] of $f = 1.68 \pm 0.23$). Hence, lines for CH_3D were scaled in strength by 2.96/5. For the foreign-broadened line widths, we used J-dependent H_2- and He-broadened widths[30], to which we fitted a 4th-order polynomial in J, using the widths calculated for $J = 13$ for higher values of J to prevent inaccurate extrapolation[31,32]. We assumed temperature dependence coefficients of these foreign-broadened widths for H_2-broadening[33] and He-broadening[35]. For the line shape, we used a Voigt function, but with sub-Lorentzian correction far from line centre as recommended for H_2-broadening conditions[36]. However, we also tested the sub-Lorentzian corrections suggested for Titan spectra[37] and a sub-Lorentzian correction previously suggested for modelling Uranus spectra[38]. Using these three different line shapes we took account of all lines within 250 cm^{-1} of each calculation wavelength.

Spectroscopic line data for hydrogen sulphide (H_2S) and ammonia (NH_3) were taken from HITRAN2012[15]. The line widths and their temperature exponents were also taken from the foreign-broadened data listed in HITRAN2012. For H_2S these are $\gamma_{air} = 0.074$ cm^{-1} atm^{-1} and a temperature exponent of 0.75, for all lines. HITRAN2012 note that detailed laboratory investigations are needed to characterise how the line widths vary with the ro-vibrational quantum number, and there appears to be no published evidence on the appropriate values for an H_2/He-broadening atmosphere. Similarly, for NH_3, we used the published HITRAN2012 foreign-broadening parameters. If the absorption of NH_3 had proved to be significant, we might have attempted to use line-broadening parameters more suited to H_2/He-broadening conditions. However, as reported in our paper, the absorption of NH_3 was not detected in these observations and hence there was no error introduced by using the listed HITRAN2012 air-broadened widths. We also examined using ExoMOL line data for H_2S[39] and found negligible differences in the spectra computed at Gemini/NIFS resolution with the HITRAN2012 line data. Since the HITRAN2012 line data are much easier to handle (they contain far fewer 'hot lines', which are only relevant for high-temperature calculations) and probably have better constrained line frequencies, we decided to use HITRAN2012 for both NH_3 and H_2S line data. In both cases, in the absence of any better information and in the expectation of weak absorptions (for which the exact line widths are less important), we used the published HITRAN2012 air-broadened widths and a Voigt line shape, with a line wing cut-off of 35 cm^{-1} to account for typical sub-Lorentzian wing corrections.

The line data were converted to k-distribution look-up tables, or k-tables, covering the Gemini/NIFS H-band spectral range, with 20 g-ordinates, 15 pressures, equally spaced in log pressure between 10^{-4} and 10 bar, and 14 temperatures, equally spaced between 50 and 180 K. These tables were precomputed with the modelled instrument line shape of the Gemini/NIFS observations, set to be Gaussian with a full-width-half-maximum (FWHM) of 0.0003 μm, after an analysis of ARC lamp calibration spectra[2].

Observations and wavelength calibration Observations of Uranus were made with Gemini-North's Near-infrared Integral Field Spectrometer (NIFS) instrument in September 2009 and October/November 2010[16,17], with adaptive optics using Uranus' nearby moons for wavefront sensing (e.g. Ariel, Titania). NIFS' H-band spectral resolution gives a Gaussian instrument function with spectral resolution of FWHM = 0.0003 μm. The wavelength calibration provided by the standard pipeline of Gemini/NIFS was found to be not quite accurate enough to match the spectral features observed here. The assumed wavelength of sample i in the spectrum is set to $\lambda_i = \lambda_0 + (i - i_0)\lambda_1$, where i_0 is the sample number of the 'central' wavelength, and the wavelength centre and step were initially assumed to be $\lambda_0 = 1.55$ μm and $\lambda_1 = 0.000155$ μm, respectively. By comparing the measured spectrum to our initial fitted spectrum we found that we could achieve a much better fit by modifying these values to $\lambda_0 = 1.54995$ μm and $\lambda_1 = 0.00016036$ μm. We used these values in the subsequent analysis.

Uranus vertical profiles of temperature and gaseous abundance The reference temperature and abundance profile used in this study (Fig. 2) is based on the 'F1' STIS/Voyager-2 profile[3]. This profile has a deep methane mole fraction of 4%[19], and has a varying relative humidity with height above the condensation level. The He:H_2 ratio in this profile is set to 0.131 and the profile includes 0.04% mole fraction of Ne. To this profile we added abundance profiles of NH_3 and H_2S, assuming arbitrary 'deep' mole fractions (i.e. above the putative NH_4SH cloud) of 0.001 for both, and limited their abundance to not exceed the saturated vapour pressure in the troposphere as the temperature falls with height. As the abundances of these gases (and CH_4) decrease with pressure the abundance of H_2 and He is adjusted to ensure the sum of mole fractions adds to unity (keeping He:H_2 = 0.131, or equivalently 12:88); the heights are calculated from the hydrostatic equation using the local temperature, gravitational acceleration and local mean total molecular weight.

For comparison we also performed retrievals using the temperature-pressure profile determined from Spitzer observations of Uranus' mid-IR spectrum[24], again with 'deep' NH_3 and H_2S abundances of 0.001. H_2 and He were assumed to be present with a ratio 85:15, again ensuring the sum of mole fractions adds to unity at all heights.

Radiative-transfer analysis The vertical cloud structure was retrieved from the Gemini/NIFS observations using the NEMESIS[18] radiative-transfer and retrieval code. NEMESIS models planetary spectra either using a line-by-line model, or by using the correlated-k approximation[40]. For speed, these retrievals were conducted using the method of correlated-k, but we regularly checked that we obtained the same model spectra (to within error) using a line-by-line approach. To model these reflected-sunlight spectra, a matrix-operator multiple-scattering model[41] was used, with 5 zenith angles (i.e. 5 upwards and 5 downwards) and the number of required components in the Fourier azimuth decomposition determined from the maximum of the reflected or incident-solar zenith angles. The collision-induced absorption of H_2-H_2 and H_2-He was modelled with published coefficients[42–44]. Rayleigh scattering was also included for completeness, but was found to be negligible at these wavelengths.

To analyse the measured radiance spectra within our radiative transfer model we initially used the high-resolution 'CAVIAR' solar spectrum[45], which we smoothed to the NIFS resolution of $\Delta\lambda = 0.0003\mu$m. However, we found that this spectrum (and others, e.g.[46,47]) contained spurious 'Fraunhofer lines' that did not seem to correspond to features seen at these wavelengths in the Uranus spectra. We must assume that the method used to generate these 'Extraterrestrial Solar Spectra' (ESS), namely measuring the solar spectrum at the ground at various zenith angles and extrapolating to an airmass of zero, leads to small errors at these wavelengths. Hence, we used a smoothed version of the solar spectrum[47] in our calculations, omitting the spurious 'Fraunhofer lines', which we found matched our observations much more closely.

The observed spectrum (with $n_y = 937$ spectral points) was fitted with NEMESIS using a continuous distribution of cloud particles whose opacity at 39 levels spaced between ~ 10 and ~ 0.01 bar was retrieved. For this cloud profile the *a priori* opacity values (at 1.6 μm) were set to 0.001 ± 0.0005 g^{-1} cm^2 at all levels (equating to opacity/bar values of ~ 1), with a 'correlation length' of 1.5 scale heights to ensure the profile was vertically smooth. NEMESIS treats cloud opacity as log values and so the error was converted to $\pm 50\%$. The particles were assumed to have a standard Gamma size distribution with mean radius 1.0 μm and variance 0.05, which are typical values assumed in previous analyses. Using a previously published technique[21], NEMESIS was used to retrieve the imaginary refractive index spectrum of these particles. The *a priori* imaginary refractive index spectrum was sampled at every 0.05 μm between 1.4 and 1.8 μm, with a 'correlation length' of 0.1 μm set in the covariance matrix, to ensure that retrieved spectrum varied reasonably smoothly with wavelength. At each iteration of the model, the real part of the particles' refractive index spectrum was computed from the imaginary part using the Kramers-Kronig relation[48], fixing the real part of the refractive index of these particles to 1.4 at a wavelength of 1.6 μm. Self-consistent scattering properties were then calculated using Mie theory, but the Mie-calculated phase functions were approximated with combined Henyey-Greenstein functions at each wavelength to smooth-over features peculiar to perfectly spherical scatterers such as the 'rainbow' and 'glory'. This is justified since we expect the actual aerosols in the atmosphere of Uranus to be solid condensates, and thus non-spherical. However, assuming these non-spherical particles are randomly orientated with respect to each other, the bulk scattering properties, such as cross-section and single-scattering albedo, are reasonably approximated with Mie theory[34], especially if the phase functions are also modified as we describe.

Since methane is the main gaseous absorber we tested to see whether some of the approximations assumed in the WKLMC@80K+[14] line database might be having an adverse effect on our calculations. We first checked whether excluding the lines observed at 296 K, but not at 80 K (and which are assigned a lower state energy high enough to reduce the computed strength at 80 K to be below the measurement noise limit) might significantly affect the calculated spectra, but found very little difference when these lines were neglected. We also checked the effect excluding the lines observed only at 80 K as well (and which are assigned an arbitrary lower state energy of -1 cm^{-1}). In this case, the differences were larger, but on the whole the model correctly reproduced the shape and main features of the observed spectrum.

Retrieval Tests Supplementary Fig. 12 shows our fit to the Uranus spectrum, setting the *a priori* imaginary refractive indices to 0.01 ± 0.005 at all wavelengths and using the three different sub-Lorentzian line shapes for CH_4 (neglecting H_2S and NH_3 absorption). We found that each assumption for the sub-Lorentzian correction gave a very similar fit to the spectrum ($\chi^2/n \sim$ 1.7–1.9), which was initially puzzling. However, the reason for this is easy to understand from Supplementary Fig. 12. The effect of different sub-Lorentzian corrections is most apparent on the shortwave side of the strong absorption band at 1.7 – 1.8 μm and previous studies have tuned the correction to get the best match to the observed spectrum between 1.5 and 1.62 μm. Our current model, however, can very easily fit this region by varying the imaginary refractive index spectrum of the particles and it can be seen that very different imaginary refractive index spectra are retrieved for the three different sub-Lorentzian corrections, but very similar vertical cloud distributions and similar spectral fits. In other words, there is a degeneracy between the sub-Lorentzian corrections and the retrieved imaginary refractive index. In fact, we had to be careful not to allow the imaginary refractive index retrieval too much freedom. Early retrievals sampled the imaginary refractive index spectrum more finely ($\Delta\lambda = 0.005\mu$m) over the 1.56 – 1.6 μm range and significant part of the spectral variation of reflectivity was accounted for by variations in n_i, which it was difficult to justify as being realistic. We thus assumed the slow wavelength-to-wavelength variation in n_i as described. Since the line shape recommended for H_2-He atmospheres[36] gave a good fit to the observations, we chose to use this assumption in our final analysis.

Scattering Properties Since the fitted imaginary refractive index spectrum for our cloud particles has values of typically $n_i \sim 0.06$, this leads the particles to be quite absorbing. This can best be seen in Supplementary Fig. 1, where we compare the computed wavelength dependence of the extinction cross-section (normalised to 1.6 μm), the single-scattering albedo, and the asymmetry, g, of the forward part of the fitted combined Henyey-Greenstein phase functions for the case when the *a priori* imaginary refractive indices were set to 0.01 ± 0.005. We found the back-scattering part of the phase-function to be insignificant. As we can see the single-scattering albedo has values of $\varpi = 0.7 - 0.8$, while the phase function asymmetry, g, is ~ 0.7.

3 Data availability statement

The data that support the plots within this paper and other findings of this study are available from the corresponding author upon reasonable request.

4 Methods References

27. Campargue, A., Wang, L., Mondelain, D., Kassi, S., Bézard, B., Lellouch, E., Coustenis, A., de Bergh, C., Hirtzig, M. & Drossart, P. An empirical line list for methane in the 1.26 – 1.71 μm region for planetary investigations (T = 80 – 300 K). Application to Titan. *Icarus* **219**, 110 –128 (2012).

28. Feuchtgruber, H., Lellouch, E., Orton, G., de Graauw, T., Vandenbussche, B., Swinyard, B., Moreno, R., Jarchow, C., Billebaud, F., Cavalié, T., Sidher, S. & Hartogh, P. The D/H ratio in the atmospheres of Uranus and Neptune from Herschel-PACS observations. *Astron. Astrophys.* **551**, A126 (2013).

29. Lécluse, C., Robert, F., Gautier, D. & Guiraud, M. Deuterium enrichment in giant planets. *Planet. Space Sci.* **44**, 1579 – 1592 (1996).

30. Pine A. S. Self-, N_2-, O_2-, H_2-, Ar-, and He- broadening in the ν_3 band Q branch of CH_4. *J. Chem. Physics* **97**, 773 – 785 (1992).

31. Amundsen D. S., Baraffe I., Tremblin P., Manners J., Hayek W., Mayne N. J. & Acreman D. M. Accuracy tests of radiation schemes used in hot Jupiter global circulation models. *Astron.*

Astrophys. **564**, A59 (2014).

32. Garland, R. & Irwin, P.G.J., 2018. Effectively calculating gaseous absorption in radiative transfer models of exoplanetary and brown dwarf atmospheres. *Mon. Not. R. Astro. Soc.* (in preparation, 2018).

33. Margolis J. S. Hydrogen broadening and collision-induced line shifts of methane at 4200 cm^{-1}. *J.Q.S.R.T.* **49**, 71 – 79 (1993).

34. Mishchenko M. I., Travis, L. D., Khan, R.A. & West, R. A. Modeling phase functions for dust-like tropospheric aerosols using a shape mixture of randomly oriented polydisperse spheroids. *J. Geophys. Res.* **102**, 16831 – 16847 (1997).

35. Varanasi P. & Chudamani S. The temperature dependence of lineshifts, linewidths and line intensities of methane at low temperatures. *J.Q.S.R.T.* **43**, 1 – 11 (1990).

36. Hartmann, J.-M., Boulet, C., Brodbeck, C., van Thanh, N., Fouchet, T. & Drossart, P. A far wing lineshape for H_2-broadened CH_4 infrared transitions. *J.Q.S.R.T.* **72**, 117 – 122 (2002).

37. de Bergh, C., Courtin, R., Bézard, B., Coustenis, A., Lellouch, E., Hirtzig, M., Rannou, P., Drossart, P., Campargue, A., Kassi, S., Wang, L., Boudon, V., Nikitin, A. & Tyuterev, V. Applications of a new set of methane line parameters to the modeling of Titan's spectrum in the 1.58 μm window. *Planet. Space Sci.* **61**, 85 – 98 (2012).

38. L.A. Sromovsky, Fry, P.M., Boudon, V., Campargue, A. & Nikitin, A. Comparison of line-by-line and band models of near-IR methane absorption applied to outer planet atmospheres. *Icarus* **218**, 1 – 23 (2012).

39. Azzam, A. A. A., Tennyson, J., Yurchenko, S. N. & Naumenko, O. V. ExoMol molecular line lists - XVI: The rotation-vibration spectrum of hot H_2S. *Mon. Not. Roy. Ast. Soc.* **460**, 4063 – 4074 (2016).

40. Lacis, A.A. & Oinas, V. A description of the correlated-k distribution method for modelling nongray gaseous absorption, thermal emission, and multiple scattering in vertically inhomogeneous atmospheres. *J. Geophys. Res.* **96**, 9027 – 9063 (1991).

41. Plass, G.N., Kattawar, G.W. & Catchings, F.E. Matrix operator method of radiative transfer. 1: Rayleigh scattering. *Appl. Opt.* **12**, 314 – 329 (1973).

42. Borysow, A. Modeling of collision-induced infrared absorption spectra of H_2 – H_2 pairs in the fundamental band at temperatures from 20 to 300 K. *Icarus* **92**, 273 – 279 (1991).

43. Borysow, A. New model of collision-induced infrared absorption spectra of H_2 – He pairs in the 2 – 2.5 μm range at temperatures from 20 to 300 K – An update. *Icarus* **96**, 169 – 175 (1992).

44. Zheng, C. & Borysow, A. Modeling of collision-induced infrared absorption spectra of H_2 pairs in the first overtone band at temperatures from 20 to 500 K. *Icarus* **113**, 84 – 90 (1995).

45. Menang, K.P., Coleman, M.D., Gardiner, T.D., Ptashnik, I.V. & Shine, K.P. A high-resolution near-infrared extraterrestrial solar spectrum derived from ground-based Fourier transform spectrometer measurements. *J. Geophys. Res.* **118**, 5319 – 5331 (2013).

46. Fiorenza, C. & Formisano, V. A solar spectrum for PFS data analysis. *Planet. Space Sci.* **53**, 1009 – 1016 (2005).

47. Thuillier, G., Hersé, M., Labs, D., Foujols, T., Peetermans, W., Gillotay, D., Simon, P.C. & Mandel, H. The solar spectral irradiance from 200 to 2400 nm as measured by the SOLSPEC spectrometer from the ATLAS and EURECA missions. *Solar Physics* **214**, 1 – 22 (2003).

48. Sheik-Bahae. Nonlinear Optics Basics. Kramers-Kronig Relations in Nonlinear Optics. In Robert D. Guenther. *Encyclopedia of Modern Optics*. Amsterdam: Academic Press (2005).

5 Figures and Tables

Table 1: Retrieval results at all areas considered on Uranus' disc.

Area	Latitude	p_1	f_{H_2S}	χ^2/n	χ^2/n_y	$\Delta\chi^2$	x_{H_2S}	A_{H_2S}	R_H
1[a]	15.3°N	1.99	113 ± 12	1.30	1.23	367.3	0.47	2.7	2.1
2	13.8°N	2.00	134 ± 19	1.04	0.99	140.7	0.58	3.3	2.3
3	15.3°S	2.10	123 ± 16	1.23	1.17	225.1	0.80	4.9	2.5
4	32.5°N	1.88	303 ± 45	1.31	1.24	218.7	0.82	4.4	2.6
5	44.7°N	1.66	474 ± 84	1.33	1.26	172.9	0.43	2.1	2.8
6[b]	62.0°N	1.56	252 ± 211	1.31	1.24	1.8	0.13	0.6	3.9
7	4.9°N	1.98	96 ± 9	1.57	1.48	333.8	0.38	2.2	2.2
1[c]	15.3°N	2.28	16 ± 2	1.36	1.29	292.1	0.43	2.9	2.1

Notes: p_1 is the pressure(bar) where the cloud opacity to space is unity; f_{H_2S} is the retrieved H_2S relative humidity (%); χ^2/n is the reduced chi-squared statistic of the fit when H_2S is included, where $n = n_y - n_x = 889$; χ^2/n_y is the chi-squared statistic of the fit when H_2S is included, where $n_y = 937$; $\Delta\chi^2$ is how much the χ^2 of the fit reduces when H_2S absorption is included – values greater than 9 can be considered significant; x_{H_2S} is mole fraction of H_2S (ppm) at p_1; A_{H_2S} is the column amount of H_2S (10^{19} molecule cm^{-2}) above p_1; R_H is a haze 'index' – the ratio of the average radiance from 1.63 – 1.64 μm divided by the average radiance from 1.57 –1.58 μm, expressed as %.

Further notes: [a]Area 1 is the main area studied; [b]For polar area 6, where the radiance is lower, the measurement errors did not need to be multiplied by 1.6 ensure a good χ^2/n; [c]Same area a s reference, but analysed using the Spitzer temperature profile, rather than 'F1'.

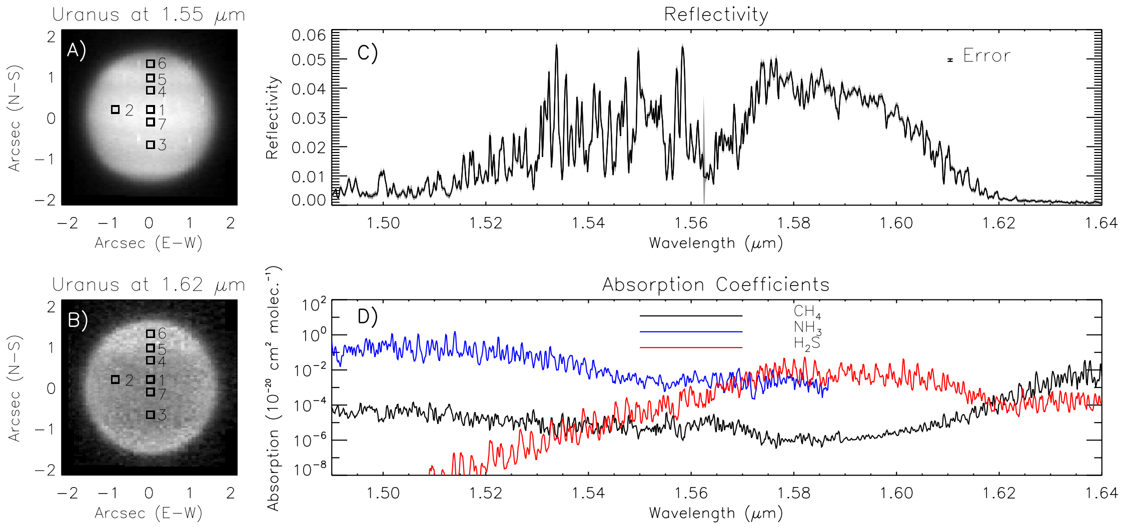

Figure 1: The appearance and spectrum of Uranus at the near-infrared wavelengths observed by Gemini/NIFS and associated absorption spectra of CH_4, NH_3 and H_2S. Panel A: The appearance of Uranus at 1.55 μm (low methane absorption, showing reflection for cloud/haze at all vertical levels), observed with Gemini/NIFS on 2nd November 2010 at approximately 06:00UT, showing the position of the seven 5×5 pixel test areas picked for retrieval analysis. Panel B: The appearance of Uranus at 1.62 μm (high methane absorption, showing reflection from upper atmospheric haze only). Panel C: Reference spectrum of Uranus[16] analysed in this study, averaged over area '1' just north of the equator, near the disc centre, with a mean latitude of 15.3°N, and error estimates shown in grey. Panel D: Mean strength listed in the k-distribution tables used in this study across the Gemini/NIFS spectral range. These absorption tables were generated from the WKLMC@80K+[14] database for CH_4, and from HITRAN2012[15] for H_2S and NH_3. These mean absorption coefficients have been computed at a temperature of 100 K and pressure of 1 atm, similar to conditions found at the tops of Uranus' main visible clouds. Note that for NH_3, the linedata in HITRAN2012 terminate at 1.587 μm, roughly half way through the H_2S absorption band.

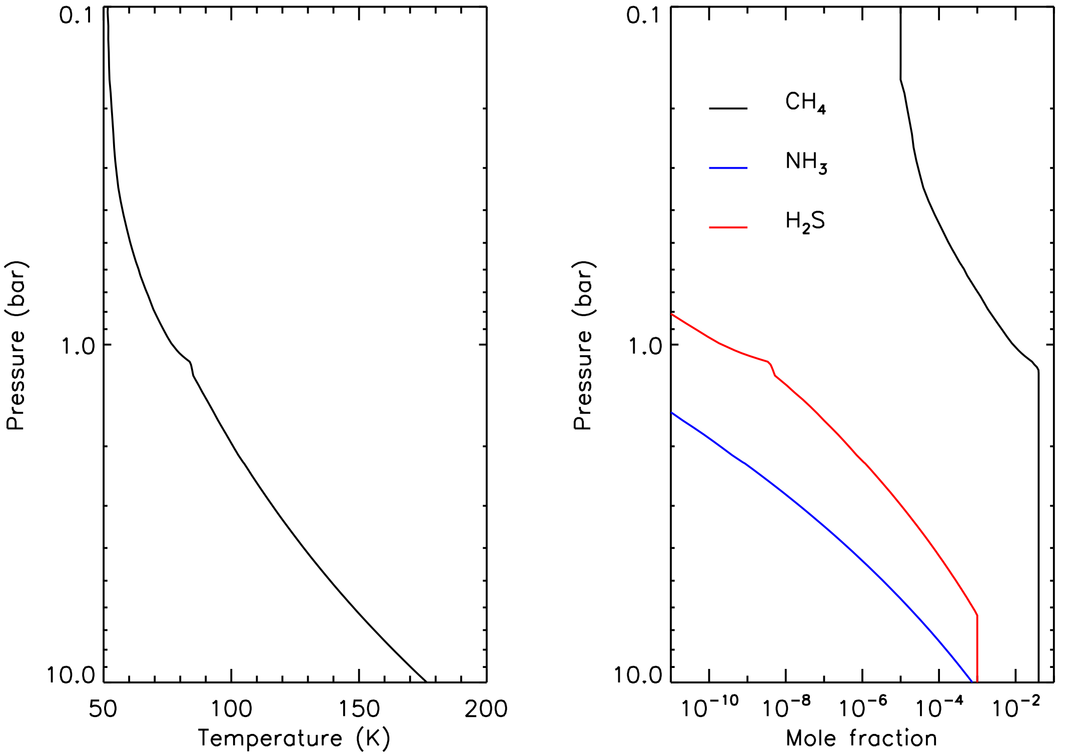

Figure 2: Assumed pressure variation of temperature (left-hand panel) and condensible abundances (right-hand panel) assumed in this study for Uranus. The temperature-pressure profile is based on the 'F1' profile[3]. The vertical variation of the CH_4 abundance is as described in the text. The abundances of NH_3 and H_2S have simply been limited by their saturation vapour pressures.

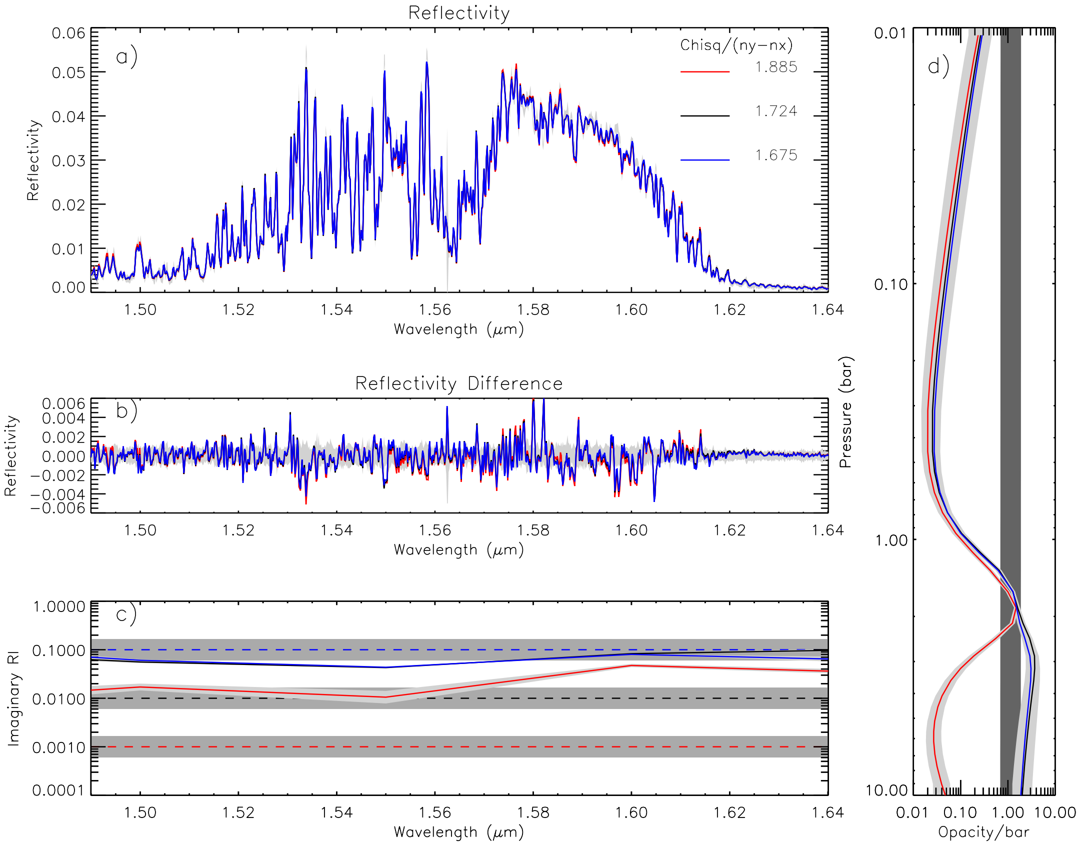

Figure 3: Fits to average Gemini/NIFS observation of Uranus, made on 2nd November 2010 at 15.3° N, using three different assumptions for the *a priori* imaginary refractive index spectrum, and excluding H_2S and NH_3 absorption. The red lines shows the results using $n_i = 0.001 \pm 0.0005$, the black lines shows the results using $n_i = 0.01 \pm 0.005$, while the blue lines show the results using $n_i = 0.1 \pm 0.05$. Panel a) shows the fits to the measured spectra, panel b) shows the difference between the observed and modelled spectra. Panel c) shows the fitted imaginary refractive index spectra of the one type of particle assumed right hand plot, while panel d) shows the fitted cloud profiles (opacity/bar at 1.6 μm). In panels c) and d) the *a priori* value and range is marked in light grey, while the error range on the retrieved quantities is indicated in darker grey. The χ^2/n of the fits is also shown in panel a).

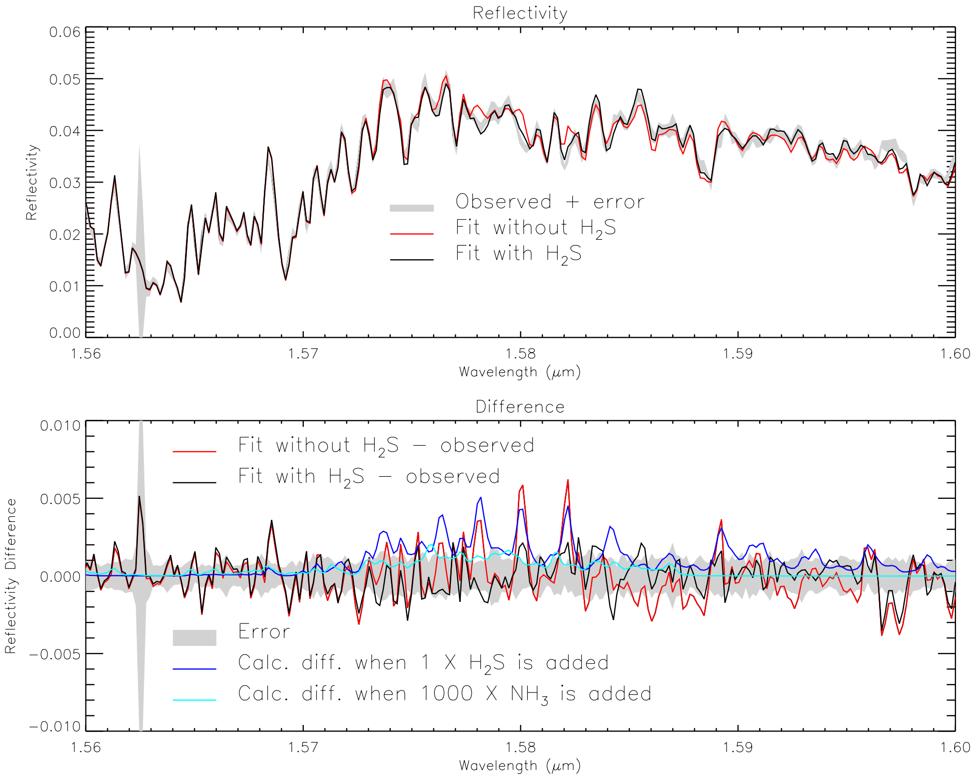

Figure 4: Fits to the co-added Gemini/NIFS observation of Uranus in the wavelength range 1.56 – 1.6 μm. In the top plot, the observed reflectivity spectrum and estimated error is shown in grey, the fitted spectrum when H_2S absorption is not included is shown in red, while the fitted spectrum when H_2S absorption **is** included is shown in black. The bottom plot shows the differences between these fits and the observed spectrum using the same colours (i.e. red when H_2S absorption is not included and black when it is), with the error range again shown in grey. The blue line in the bottom plot shows how the calculated spectrum for the fit when H_2S absorption is not included (i.e. red line in the top plot) changes when H_2S absorption is added (leaving all other fitted parameters unchanged), assuming a profile with 100% relative humidity (RH). The cyan line shows how the calculated spectrum changes when NH_3 absorption is added, leaving all other fitted parameters unchanged, assuming a profile with 1000 times the *a priori* NH_3 profile with 100% RH.